ISBN: 978-3-95450-247-9 ISSN: 2673-5490 doi: 10.18429/JACoW-IPAC2024-WEPC63

DARK CURRENT REDUCTION FOR NSRRC PHOTOINJECTOR SYSTEM BY COLLIMATOR

Yang-Jen Lin, Department of Engineering and System Science, NTHU, Hsinchu, Taiwan
Ming-Chang Chou, Wei-Yuan Chiang, Wai-Keung Lau, An-Ping Lee, NSRRC, Hsinchu, Taiwan

Abstract

The coherent THz facility developed at NSRRC delivers superradiant radiation with wavelengths ranging from 100 – 500 μm from a gap tuneable U100 planar undulator. An S-band laser-driven photocathode rf gun has been used in its 25 MeV linac system to generate a sub-picosecond high brightness relativistic electron beam via velocity bunching for emission of coherent THz radiations. However, the high accelerating field in the gun cavity is found to be the main cause of electron field emission that generates the non-negligible background current (dark current) in the system. A portion of the field emission (FE) electrons with launching conditions close to that of the main beam can be accelerated to high energies by the booster linac structure located downstream. The primary cause of excessive radiation dosage stems from the collision of these unwanted high-energy electrons with the system's vacuum vessel. In order to limit the transportation of FE electrons from rf gun to the booster linac, a collimation system will be implemented at upstream of the booster linac. In this work, the drive linac system has been modeled with 3D space charge tracking code – IMPACT-T for both main beam as well as dark current simulation. Particle transmission and energy distribution of dark current after collimation has been simulated. Trajectories of electrons at various initial positions and particle loss mechanism have also been analysed.

INTRODUCTION

NSRRC coherent terahertz facility is a superradiant undulator radiation source driven by a relativistic sub-picosecond high-brightness electron beam generated by a photoinjector [1-2]. It provides scientific users with intense undulator radiation in the wavelength range of 100–500 μm. As shown in Fig. 1, the photoinjector is mainly composed of a 2998 MHz photocathode rf gun with copper cathode being excited by a 266 nm, picosecond UV laser and a 5.2-meter, 2998 MHz constant gradient traveling-wave linac section (booster linac) for beam acceleration to the designed energy. The system is also equipped with solenoid magnets to compensate emittance growth due to linear space charge [3]. In order to generate superradiant THz radiations, the beam is compressed to sub-picosecond in duration via velocity bunching by operating the booster linac near zero-crossing rf phase [4]. In fact, a bunch 250 pC of charge with 240 fs duration and 25 MeV beam energy has been achieved in our photoinjector system. However, system operation has been hindered by excessive ionization radiation which stems from the collision of unwanted high-energy electrons with the vacuum vessel. High accelerating field in the gun cavity is found to be the main cause of field emission that contribute free electrons to the dark current in the system. It is obvious that those FE electrons with launching conditions close to that of the main beam are most likely accelerated to high energies by the booster linac.

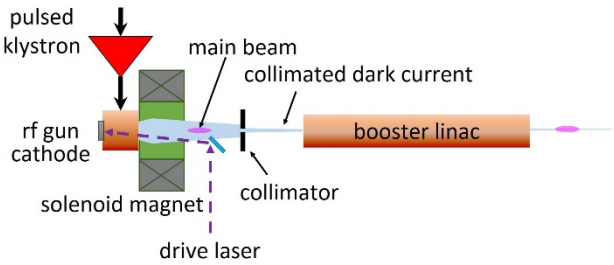

Figure 1: Schematic layout of the NSRRC photoinjector with a collimator installed to mitigate the entry of field-emitted electrons from the rf gun into the booster linac.

Due to the broad energy range of electrons in the dark current and considering the different focusing strengths of the gun solenoid for electrons of different energies, it is feasible to incorporate a collimator with a finite aperture size along the beam path to limit dark current from entering the booster linac. In this study, the dynamics of FE electrons from cathode surface has been simulated with IMPACT-T [5]. To evaluate the effectiveness of the collimator to block dark current from entering the booster linac, an initial distribution of FE electrons has been defined on the end-wall of the cavity half-cell (i.e. cathode surface) according to Fowler-Nordheim (FN) theory [6-7] and the evolution of these electrons are tracked along the photoinjector. It is worth noting that field emission from inner surfaces of gun cavity other than the half-cell end wall has been neglected because electrons emitted from these surfaces are not likely accelerated to higher energies [8-9]. On the other hand, we assume charge density of dark current is low enough such that space charge effect can be neglected in IMPACT-T simulation. The particle loss mechanism in the system has been analysed by looking into the trajectories of electrons under various initial radial and longitudinal positions. The collimator considered in this study is placed at 1.05 m away from cathode surface because it is dictated by available space in the system setup.

INITIAL FE ELECTRON DISTRIBUTION

For field emission, electrons in a metal tunnel through the potential barrier setup between the metal surface and vacuum provided that strong enough external electric field has been applied onto the surface. The emission current density j on a metallic surface depends not only on the applied electric field, but also on the intrinsic properties and

ISBN: 978-3-95450-247-9 ISSN: 2673-5490 doi: 10.18429/JACoW-IPAC2024-WEPC63

surface condition of the metal. It can be described by Fowler-Nordheim equation as [6-7]:

$$j = 1.54 \times 10^{-6} \cdot 10^{4.52\phi^{-0.5}} a_e \frac{\beta^2 E^2}{\phi} \exp\left(-\frac{6.53 \times 10^9 \phi^{1.5}}{\beta E}\right) [A/m^2]$$

where ϕ is the work function of the material in eV, E the local electric field applied on the metal surface in V/m, β the field enhancement factor and a_e the ratio of effective emission area to actual area. In an rf accelerating structure, time-harmonic field characterized by both amplitude and phase is applied on the inner surfaces of the structure.

A distribution of hundred thousand electrons in polar coordinates, shown in Fig.2, has been used to study dark current transportation in the photoinjector with and without collimator. Assuming zero momentum spread, transverse distribution of field emission electrons is determined by the current density defined by FN equation which depends on the gun cavity field distribution on cathode surface. The axis-symmetric field of our 2998 MHz, 1.6-cell rf gun cavity has been calculated by 2D electromagnetic simulation code – SUPERFISH [10]. Peak on-axis electric field is set at 60 MV/m. Typical values of β at 100 and a_e of 10^{-13} have been chosen in this study [11-12]. Due to the periodicity of rf field, while electrons are emitted from the metal surface at one half cycle, emission is cut off for the other half. For simplicity in this preliminary study, we tentatively consider electrons are distributed uniformly in an initial longitudinal position range such that the rf phase seen by the first particle as it leaves the cathode differs from that seen by the last particle by 90 degrees.

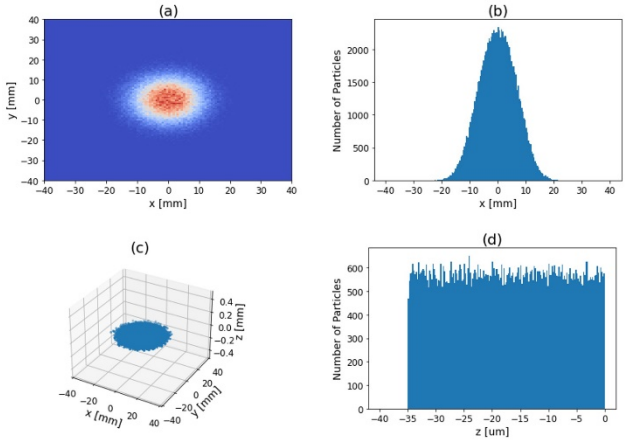

Figure 2: (a) transverse (b) horizontal (c) 3D and (d) longitudinal distribution of field emission electrons from cathode surface are defined in this study when 60 MV/m on-axis electric field is applied. Field enhancement factor β and the ratio of effective emission to actual area a_e was tentatively set at 100 and 10^{-13} respectively.

TRAJECTORIES OF FE ELECTRONS

By optimizing of the rf phases of accelerating structures (i.e. rf gun and booster linac) and solenoid magnetic fields, a high brightness sub-picosecond electron beam is generated in the photoinjector system via velocity bunching. In this IMPACT-T simulation study, the on-axis accelerating field on rf gun cathode is 60 MV/m. For minimization of transverse beam emittance at linac exit, gun rf phase and solenoid magnetic field are set at 205° and 0.118 T respectively. Under this operation condition, due to the finite sizes of gun apertures, it can be shown that not all electrons emitted from the cathode can be accelerated successfully and leave the rf gun. To study this, we performed single particle tracking calculations for electrons with different radial and longitudinal positions on cathode surface.

Figure 3 depicts results of single particle tracking with IMPACT-T for electrons with initial radial positions ranging from 0.5 to 12 mm from the centre of cathode. As shown in Fig. 3, off-centred FE electrons are deflected radially from cavity axis with initial radial positions larger than ~3 mm are blocked by either by the inter-cell or the gun exit apertures. Electrons with radial positions smaller than ~3 mm leave the rf gun successfully propagate to downstream. However, due to the broad energy range of these electrons, the gun solenoid at fixed field setting have different focusing strengths to electrons of different energies. A collimator with a finite aperture size can be inserted at a distant from the cathode along the beam path to limit dark current from entering the booster linac. We decided to put the collimator at 1.05 m away from the cathode in our case.

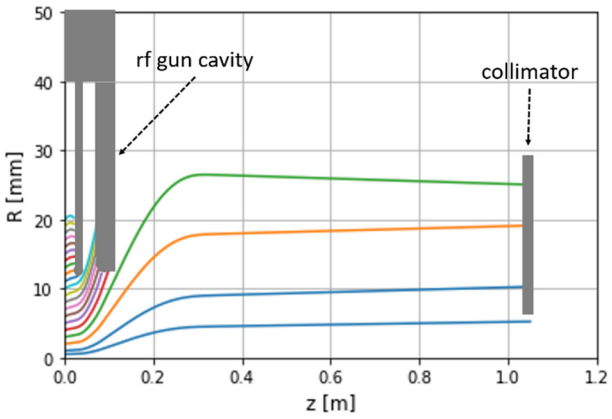

Figure 3 : Plots of trajectories of electrons with different initial radial positions on cathode surface.

For FE electrons with different initial longitudinal positions, they see different rf phases as they leaves the cathode surface according to their initial positions and averaged initial velocity v_0. The rf phase difference $\Delta\phi$ between an arbitrary particle and the leading particle is given by $\omega\Delta z/v_0$, where Δz is the difference in initial longitudinal positions. Figure 4 depicts trajectories of electrons with various initial longitudinal positions (expressed as rf phase difference between some electron and a leading electron). It is found that only those particles having rf phase differences in the range between -40 and -120 degrees (or equally 240-320 degrees) can be accelerated and propagate to downstream. For the uniform longitudinal distribution of initial FE electron we previosuly defined, some particle loss on cathode surface is expected.

ISBN: 978-3-95450-247-9 ISSN: 2673-5490 doi: 10.18429/JACoW-IPAC2024-WEPC63

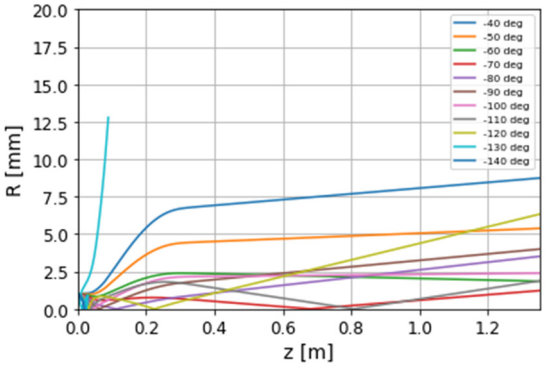

Figure 4: Trajectories of electrons with various initial longitudinal positions (expressed as rf phase difference between some electron and a leading electron).

EFFECTS OF COLLIMATOR

According to IMPACT-T simulation results, RMS size σ_r of main beam is 0.75 mm at the collimator location. Collimator aperture size of $6\sigma_r$ (i.e. 4.5 mm) is therefore taken as the minimum value without interrupting the main beam. With the distribution of hundred thousand initial FE electrons described in previous section, particle loss in photoinjector with and without a collimator with square aperture size of 4.5 mm (i.e. 4.5×4.5 mm^2 in area) have been simulated. The results are shown in Fig. 5. It is found that percentage of FE electrons that can be transmitted through the collimator can be as low as 7.12%. It is worth noting that particle loss before collimator has been observed. Since we have assumed a uniform longitudinal distribution in this preliminary study, it is not surprising to have particle loss on cathode. As explained in previous section, a significant portion of the FE electrons are blocked by the gun apertures. In this simulation, the sizes of computational domain in X- and Y- directions have been set to 40 mm. Particles that move beyond the computational domain are considered to be lost in the beamline.

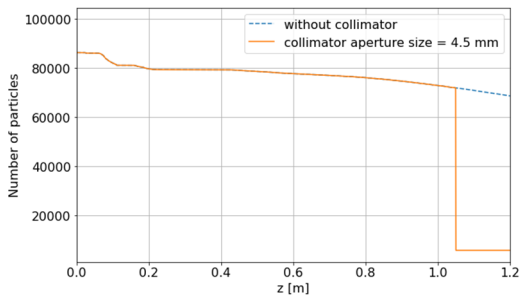

Figure 5: Simulated particle loss in photoinjector with and without a collimator with square aperture size of 4.5 mm.

Percentage of FE electrons being transmitted through the collimator aperture as a function of aperture size is calculated and plotted in Fig. 6. Particle loss is still significant even for larger aperture sizes. For example, only one third of the FE electrons survived with collimator aperture size of 16 mm. This demonstrates the effectiveness of this dark current reduction scheme.

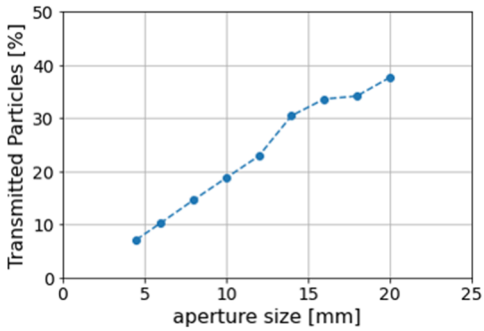

Figure 6: Percentage of FE electrons being transmitted through the collimator aperture as a function of aperture size.

To understand the energy distributions FE electrons before and after collimator, energy spectra are compared for a collimator of 6 mm aperture size. The distribution of FE electron energies is broad before collimation. But after collimation, only electrons with highest energy remain. It is believed that these remained high energy particles have properties very similar to the main beam.

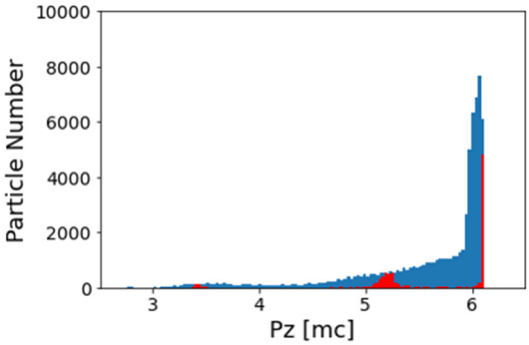

Figure 7: Electron energy spectra at booster linac entrance with(blue) and without(red) insertion of a 6 mm collimator.

CONCLUSIONS

According to FN theory, a distribution of field emitted electrons has been defined to study dark current transportation in the photoinjector with and without collimator. The effectiveness of this dark current reduction scheme has been demonstrated. to reduce It has been demonstrated the effectiveness of this dark current reduction scheme. Particle loss on collimator is still significant even for larger aperture sizes. It is very likely that the main beam will not be intercepted with proper choice of collimator aperture size.

ACKNOWLEDGEMENTS

The authors express their gratitude to Dr. Ji Qiang (LBNL) for his insightful discussions and valuable guidance regarding the utilization of the IMPACT code in this study.

REFERENCES

[1] M. C. Chou *et al.*, "Experimental Study of Coherent THz Sources Driven by the NSRRC High Brightness Photo-in-

ISBN: 978-3-95450-247-9 ISSN: 2673-5490 doi: 10.18429/JACoW-IPAC2024-WEPC63

jector", in *Proc. IPAC'18*, Vancouver, Canada, Apr.-May 2018, pp. 4332-4335.
doi:10.18429/JACoW-IPAC2018-THPMK017

[2] W. K. Lau *et al.*, "Properties of superradiant spontaneous THz undulator radiation by an RF compressed electron beam", in *Proc. IPAC'23*, Venice, Italy, May 2023, pp. 1877-1880.
https://doi.org/10.18429/JACoW-IPAC2023-TUPL055

[3] B. E. Carlsten, "Space-charge-induced emittance compensation in high-brightness photoinjectors", *Particle Accelerators*, Vol. 49, pp. 27-65, 1995.

[4] L. Serafini, "Velocity bunching in photo-injectors", *AIP Conference Proceedings*. AIP, 2001.
doi:10.1063/1.1401564

[5] J. Qiang *et al, PRST-AB* 9, 044204, 2006; J. Qiang, "IMPACT-T user document ver. 2.2", 2022.
https://github.com/impact-lbl/IMPACT-T

[6] J. W. Wang and G. A. Loew, "Field emission and rf breakdown in high-gradient room temperature linac structures", SLAC-PUB-7684, 1997.

[7] R.H. Fowler and L. Nordheim, "Electron Emission in Intense Electric Fields", *Proc. Roy. Soc. A*, 119, pp. 173-181, 1928.
doi:10.1098/rspa.1928.0091

[8] G. Shu *et al*., "Dark current studies of an L-band normal conducting RF gun", Nuclear Inst. and Methods in Physics Research, A 1010, 165546, 2021.
doi.10.1016/j.nima.2021.165546

[9] J. Qiang and K. Hwang, "Modeling of dark current generation and transport using the IMPACT-T Code", *Proc. NA-PAC'16*, Chicago, USA, pp. 964-966, 2016.

[10] J. H. Billen and L. M. Young, "POISSON/SUPERFISH on PC compatibles", *Proc. PAC'93*, Washington, DC, USA, 1993, pp. 790-792.
doi:10.1109/PAC.1993.308773.

[11] S. Bettoni *et al*., "Dark current transport and collimation studies for SwissFEL", *Proc. FEL'13*, New York, USA, 2013, pp. 209-213.
https://www.dora.lib4ri.ch/psi/islandora/object/psi:24557.

[12] S. Bettoni *et al*., "Low energy dark current collimation system in single-pass linacs", PRST-AB 21, 023401, 2018.
doi:10.1103/PhysRevAccelBeams.21.023401.